European Journal of Pharmaceutics and Biopharmaceutics 71 (2009) 71–79

Contents lists available at ScienceDirect

European Journal of Pharmaceutics and Biopharmaceutics

journal homepage: www.elsevier.com/locate/ejpb

Research paper

Better understanding of dissolution behaviour of amorphous drugs by *in situ* solid-state analysis using Raman spectroscopy

M. Savolainen [a,*], K. Kogermann [a,b], A. Heinz [c], J. Aaltonen [a,d], L. Peltonen [a], C. Strachan [d], J. Yliruusi [a]

[a] *Division of Pharmaceutical Technology, Faculty of Pharmacy, University of Helsinki, Helsinki, Finland*
[b] *Department of Pharmacy, University of Tartu, Estonia*
[c] *School of Pharmacy, University of Otago, New Zealand*
[d] *Centre for Drug Research (CDB), Faculty of Pharmacy, University of Helsinki, Helsinki, Finland*

ARTICLE INFO

Article history:
Received 11 February 2008
Accepted in revised form 4 June 2008
Available online 12 June 2008

Keywords:
Amorphous
Raman spectroscopy
Dissolution testing
Phase transformation
Partial least squares discriminant analysis (PLS-DA)
Partial least squares (PLS) regression analysis

ABSTRACT

Amorphous drugs have a higher kinetic solubility and dissolution rate than their crystalline counterparts. However, this advantage is lost if the amorphous form converts to the stable crystalline form during the dissolution as the dissolution rate will gradually change to that of the crystalline form. The purpose of this study was to use *in situ* Raman spectroscopy in combination with either partial least squares discriminant analysis (PLS-DA) or partial least squares (PLS) regression analysis to monitor as well as quantify the solid-phase transitions that take place during the dissolution of two amorphous drugs, indomethacin (IMC) and carbamazepine (CBZ). The dissolution rate was higher from amorphous IMC compared to the crystalline α- and γ-forms. However, the dissolution rate started to slow down during the experiment. *In situ* Raman analysis verified that at that time point the sample started to crystallize to the α-form. Amorphous CBZ instantly started to crystallize upon contact with the dissolution medium. The transition from the amorphous form to CBZ dihydrate appears to go through the anhydrate form I. Based on the PLS analysis the amount of form I formed in the sample during the dissolution affected the dissolution rate. Raman spectroscopy combined with PLS-DA was also more sensitive to the solid-state changes than X-ray powder diffraction (XRPD) and was able to detect changes in the solid-state that could not be detected with XRPD.

1. Introduction

Different solid-state forms of a drug, such as crystalline, amorphous, or hydrate forms, have different physical, chemical and mechanical properties [1–3]. These properties not only affect the processability and stability of the drug product but can also lead to differences in bioavailability. Thus, the choice of the solid-state form offers a way to alter, for example, dissolution properties during formulation development. An increasing number of the new drug candidate molecules are poorly water soluble. Thus, there is a growing interest in formulation approaches to improve the dissolution rate of these drugs. The use of drugs in an amorphous form is often mentioned as a possibility to improve the solubility and dissolution rate of poorly water soluble drugs, since a several fold increase in solubility can be obtained when using amorphous forms instead of their crystalline counterparts [4].

The amorphous state is a high-energy state compared to the crystalline state and, thus, the solubility and dissolution rate are higher for the amorphous form [2,5]. However, due to the metastable nature of amorphous drugs, they tend to crystallize. The underlying mechanism behind the crystallization can be either a solid-state or solution-mediated transformation and both these transformation mechanisms involve first a nucleation phase before crystal growth can occur [2,6]. Molecular mobility can increase in the solid phase due to either an increase in temperature or by the sorption of water into the sample. Sorption of water into the sample will decrease the glass transition temperature (T_g) and plasticize the sample. The molecular mobility is higher on the surface than in the bulk and, therefore, the surface crystallization rate of an amorphous solid is faster than the bulk crystallization rate [7,8]. A solution-mediated transformation, on the other hand, requires a supersaturated solution. The dissolved drug would, thus, recrystallize on the surface as a more stable crystalline form. These phase transformations have a significant impact on the dissolution rate, since even a thin layer of crystalline material on the surface would change the dissolution rate of the drug to that of the crystalline form.

Crystallization of the amorphous form can occur either during manufacturing, storage or in the body upon contact with the gastrointestinal fluids. In order for the amorphous formulation approach to succeed, it is not enough that the drug remains in

* Corresponding author. Division of Pharmaceutical Technology, Faculty of Pharmacy, P.O. Box 56, FI-00014, University of Helsinki, Finland. Tel.: +358 9 191 59159; fax: +358 9 191 59144.
E-mail address: marja.savolainen@helsinki.fi (M. Savolainen).

0939-6411/$ - see front matter © 2008 Elsevier B.V. All rights reserved.
doi:10.1016/j.ejpb.2008.06.001

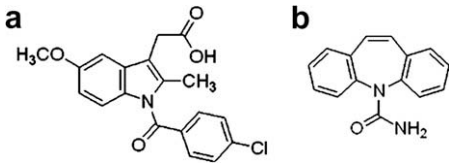

Fig. 1. Structural formula of (a) IMC and (b) CBZ.

the amorphous form for the entire storage time but it must remain amorphous also during dissolution. Several factors affect the degree of solubility and dissolution enhancement obtained from the amorphous form compared to the crystalline counterparts, such as the amorphous to crystalline transformation mechanism (solid-state mediated, solution-mediated or combination of both) [9]. Overall, the observed experimental dissolution behaviour of the metastable form is related to the solubility and dissolution rate of the metastable form, the conversion rate to the stable form and the solubility and dissolution rate of the stable form [10]. Thus, the conversion rate of the metastable amorphous form to the stable crystalline form has to be lower than the dissolution rate of the metastable form, otherwise the dissolution rate will gradually change towards that of the stable crystalline form.

Previous studies have looked at the dissolution behaviour of amorphous drugs and accompanying solid-state transitions [11,12]. However, in these studies information about the phase transformations is obtained by analyzing the sample off line after the experiment. Therefore, no information about the transition pathway is obtained. To our knowledge, there are no studies that have looked at the solid-state transitions *in situ* during dissolution testing of amorphous materials. Our aim was to use *in situ* Raman spectroscopy to gain understanding of the solid-state changes that might occur during the dissolution testing of two amorphous model substances: indomethacin (IMC) and carbamazepine (CBZ) (Fig. 1). Furthermore, the aim was to combine Raman spectroscopy with multivariate analysis (partial least squares discriminant analysis (PLS-DA) and partial least squares regression (PLS) analysis) to improve the interpretation of the spectroscopic data. PLS analysis was used to quantify the amount of different solid-state forms present during the dissolution experiments.

2. Materials and methods

2.1. Materials

γ-Indomethacin (USP grade) was used as obtained from the manufacturer (Hawkins, Inc., Minneapolis, MN, USA). α-Indomethacin was prepared by dissolving γ-IMC in hot ethanol and subsequently adding distilled water causing α-IMC to precipitate [13].

Carbamazepine (form III, USP grade) was purchased from Hawkins, Inc. (Minneapolis, MN, USA). Form I was prepared by heating the raw CBZ form III at 170 °C at atmospheric pressure for 2 h [14]. The dihydrate was recrystallized by slow cooling of hot (80 °C) saturated aqueous solution to room temperature. The solution was slowly cooled to room temperature. After vacuum filtration the crystals were dried at ambient conditions and stored at room temperature at 54% RH.

2.2. Preparation of samples for PLS calibration

PLS calibration samples were prepared by gently mixing the four forms of CBZ (dihydrate, form I, form III and amorphous) in different weight ratios [15]. To reduce sample inhomogeneity caused by particle size differences, all forms were gently ground using a mortar and pestle and then sieved to obtain a particle size of less than 0.8 mm. The solid-state of the samples after grinding and sieving was verified by XRPD. The mixture ratios were selected based on a quaternary mixture design constructed in Modde (Version 7.0.0.1, Umetrics AB, Umeå, Sweden). An axial extended linear model was developed. The model consisted of 12 mixtures in triplicate with concentrations of 100%, 62.5%, 33.3%, 12.5%, and 0% for each component and nine samples consisting of 25% of each form as centre point mixtures. All mixtures were stored in closed glass vials and the measurements were performed on the day of preparation.

2.3. Preparation of samples for dissolution experiments

Powder compacts of crystalline α- and γ-IMC, as well as, CBZ dihydrate were compressed with a single punch tablet machine (Korsch EK0, Erweka Apparatebau, Germany) using flat-faced punches with a diameter of 9 mm. The mass of the compacts was 150 mg and they were compressed to a crushing strength of 50 N for IMC and 40 N for CBZ dihydrate. The amorphous samples were prepared by melting γ-IMC and CBZ (form III) and pouring the melt into a circular mold with a diameter of 9 mm. The samples were then cooled to room temperature over phosphorus pentoxide (P_2O_5).

2.4. Dissolution testing

Dissolution tests were carried out in a channel flow intrinsic dissolution test apparatus with a quartz sight window for the Raman probe, where only one surface of the sample is in contact with the dissolution medium [16]. Phosphate buffer solution of pH 7.2 at room temperature was used as the dissolution medium for both IMC and CBZ. For IMC, a water–ethanol (50% (w/w)) solution in which IMC exhibits a higher solubility was also used as the dissolution medium as proof-of-principle, since both the dissolution rate and the amount of crystalline IMC appearing on the surface were low in the phosphate buffer solution. The flow rate of the solution was 8 ml/min. The amount of dissolved drug in the dissolution medium was determined using a UV–vis spectrophotometer (Ultrospec III, Pharmacia LKB Biotechnology, Sweden) with a flow-through cuvette at wavelengths of 288 nm (CBZ) and 318 nm (IMC). The absorbance values were collected at intervals of 10 s. The IMC dissolution experiments lasted for five hours in the buffer solution and for one hour in the 50% water–ethanol solution. The CBZ tests were carried out in phosphate buffer (pH 7.2) for two hours. All the dissolution tests were done at least in triplicate.

2.5. In situ solid-state analysis using Raman spectroscopy

The solid-state of the sample surface was analyzed *in situ* through a quartz sight window using a Raman spectrometer (Control Development Inc., South Bend, IN, USA) equipped with a thermoelectrically cooled CCD detector and a fibre optic probe (spot size 200 μm, focal length 10 mm; InPhotonics, Norwood, MA, USA). The measurements were carried out at room temperature using a 500 mW laser source with a wavelength of 785 nm (Starbright 785 S, Torsana Laser Technologies, Skodsborg, Denmark). The integration time for IMC and CBZ samples was 2 s and 1 s, respectively. Each spectrum was the average of five scans. During the dissolution experiments, IMC spectra were collected with an interval of 60 s in phosphate buffer and 30 s in water–ethanol solution. CBZ spectra were recorded every 15 s. To decrease the effect of fluorescence on the Raman spectra the amorphous IMC samples were photochemically bleached for 15 min immediately before the dissolution experiment.

2.6. X-ray powder diffraction (XRPD)

The solid-state of the compacts and the glassy samples was analyzed with an X-ray powder diffractometer (D8 Advance, Bruker AXS GmbH, Karlsruhe, Germany). The diffraction patterns were recorded using a theta-theta XRPD equipped with Göbel mirror bent multilayer optics. Measurements were performed in symmetrical reflection mode with CuKα radiation ($\lambda = 1.54$ Å) at 40 kV and 40 mA. The samples were scanned in the angular range of 5° to 40° 2θ with a step size of 0.1° and a count time of 5 s per step for IMC. For CBZ, an angular range of 5° to 30° 2θ with a step size of 0.1° and a count time of 3 s per step was used. The samples were analyzed before and after dissolution testing to confirm the solid-state of the samples.

The experimental diffraction patterns were compared to the theoretical ones based on the crystal structures obtained from the Cambridge Structural Database (CSD). INDMET02 and INDMET03 were used as reference structures for α- and γ-IMC, respectively [17,18]. For the theoretical diffraction patterns of CBZ form I, form III, and dihydrate the respective refcodes CBMZPN11, CBMZPN01 and FEFNOT02 were used [19–21].

2.7. Data analysis

2.7.1. Partial least squares discriminant analysis (PLS-DA)

PLS-DA is based on partial least squares (PLS) regression analysis, where two data matrices **X** (variables, e.g. spectra) and **Y** (responses, e.g. solid-state forms) are correlated to each other [22]. PLS-DA is, thus, used to semiquantitatively discriminate between different classes of observations. Principal component analysis (PCA) is usually performed for qualitative purposes. In PCA, the scores and the loadings are the projection of the matrix **X**. The scores are new variables that summarize the information from the original variables, and loadings describe how the variable influences the component. In PLS-DA, PCA is performed on both the matrices and then the best possible correlation between the matrices is determined using the least squares technique. PLS-DA enables the rotation of the components such that the maximum separation among classes is obtained and the covariance between the scores and the weights of the matrices **X** and **Y** is maximized. PLS-DA was carried out using Simca-P software (v. 10.5, Umetrics ab, Umeå, Sweden). Pure samples of the amorphous and crystalline forms were used for calibration. The samples were measured at least in triplicate, separate from the dissolution experiments. Before PLS-DA, both IMC and CBZ spectra were corrected using standard normal variate transformation (SNV) [23] and mean centring. The spectral regions chosen for the analysis of IMC samples were 1085 to 1480 cm^{-1} and 1560 to 1690 cm^{-1}. For CBZ, the spectral region of 1200 to 1680 cm^{-1} was used. A more detailed description of the CBZ model development can be found in a paper by Kogermann et al. [24].

2.7.2. Partial least squares (PLS) regression analysis

In PLS regression analysis the **X** matrix (variables, e.g. spectra) is correlated with a **Y** matrix (responses, e.g. concentrations) [22]. PLS regression analysis was used to extract quantitative information from the spectroscopic data measured during the CBZ dissolution tests. PLS analysis was carried out using Simca-P software (v.10.5, Umetrics ab, Umeå, Sweden). The pure samples of the crystalline (form I, form III and dihydrate) and the amorphous forms of CBZ, as well as the mixtures of these in different weight ratios, were measured at least in triplicate separate from the dissolution experiments. A more detailed description of the model development can be found in a paper by Kogermann et al. [15]. Two thirds of the data were randomly selected and used to create the model and the remaining third to validate the model. The spectral region of 1208 to 1691 cm^{-1} was chosen for the analysis. Before PLS analysis, the CBZ spectra were SNV corrected [23] and mean centred.

3. Results and discussion

3.1. Indomethacin

3.1.1. Dissolution experiments

XRPD analysis of the samples showed that all samples were amorphous after preparation (Fig. 2). In the beginning of the intrinsic dissolution experiments, the dissolution rate from the amorphous IMC samples was faster than from the crystalline counterparts (Figs. 3a and 4a) [11,13,25,26]. However, the dissolution rate started to decrease after less than two minutes in water–ethanol solution, and at the end of the experiment the dissolution rate resembled that of the α-IMC. In phosphate buffer, the dissolution rate gradually decreased after the first 30 min below the dissolution rates of the crystalline forms.

Amorphous IMC is yellow, whereas both the crystalline forms are white. Visual inspection of the sample surface before and after dissolution testing showed that the clear yellow surface of the amorphous sample had turned opaque and the surface was partly covered with white crystalline IMC. More white crystals could be noted on the samples that had been in the water–ethanol solution compared to the sample in phosphate buffer. The XRPD analysis of the sample surface after the dissolution experiment showed that the crystals formed on the surface of the sample in water–ethanol solution were of the α-polymorph (Fig. 2). In phosphate buffer solution, the amount of crystalline IMC on the surface was so small that it could not be detected with XRPD.

3.1.2. Monitoring the solid-state transformations

Small changes could be noted in the Raman spectra that had been measured *in situ* in both dissolution media. However, in the case of IMC the differences between the Raman spectra of the amorphous and the crystalline forms are small; only some merging of the peaks, decrease in peak intensities and broadening of bands can be noted [27,28]. This makes the interpretation of the spectra difficult. The advantage of multivariate analysis, such as PLS-DA, is that all the spectral information and not just a couple of peaks can be used for the analysis. Therefore, to obtain further understanding of the phenomena that occur during dissolution, PLS-DA analysis of the Raman spectra was carried out.

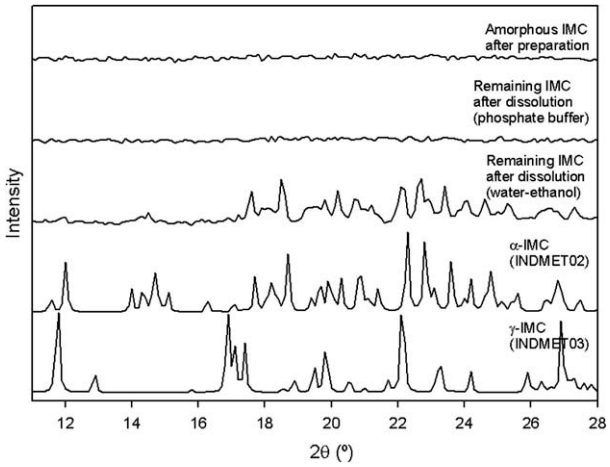

Fig. 2. XRPD patterns of the originally amorphous IMC samples before and after the dissolution experiments and the theoretical diffraction patterns of the crystalline forms.

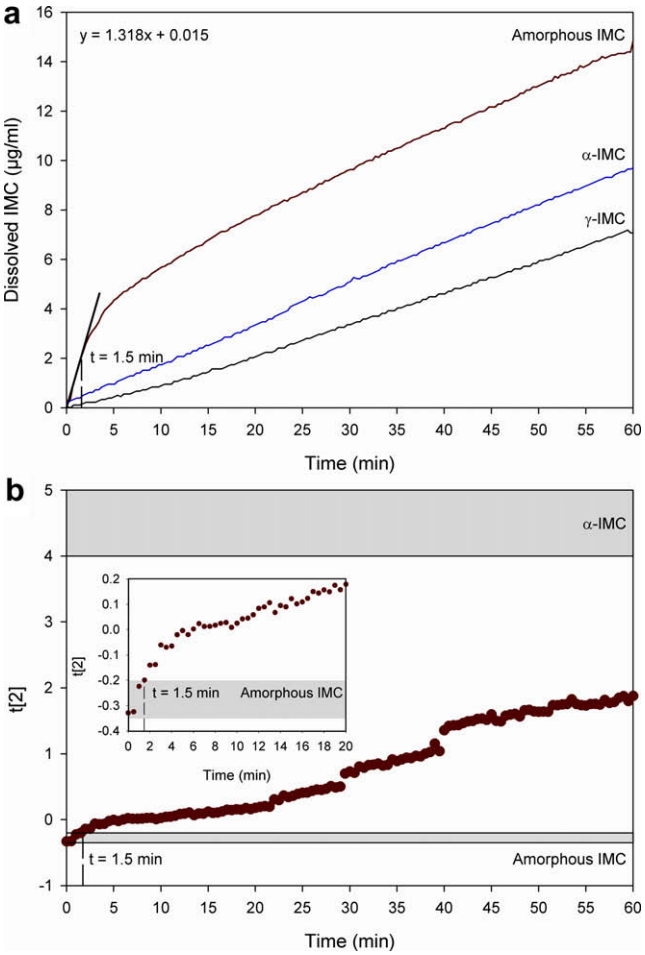

Fig. 3. (a) Dissolution of IMC in the water–ethanol (50% (w/w)) solution and (b) the respective scores of the amorphous sample following the PLS-DA. The grey areas represent the score regions (the area between smallest and largest score value) of amorphous IMC and the crystalline α-IMC. The maximum standard deviation in concentrations is 0.5 µg/ml. The equation refers to the line of fit for the initial dissolution profile.

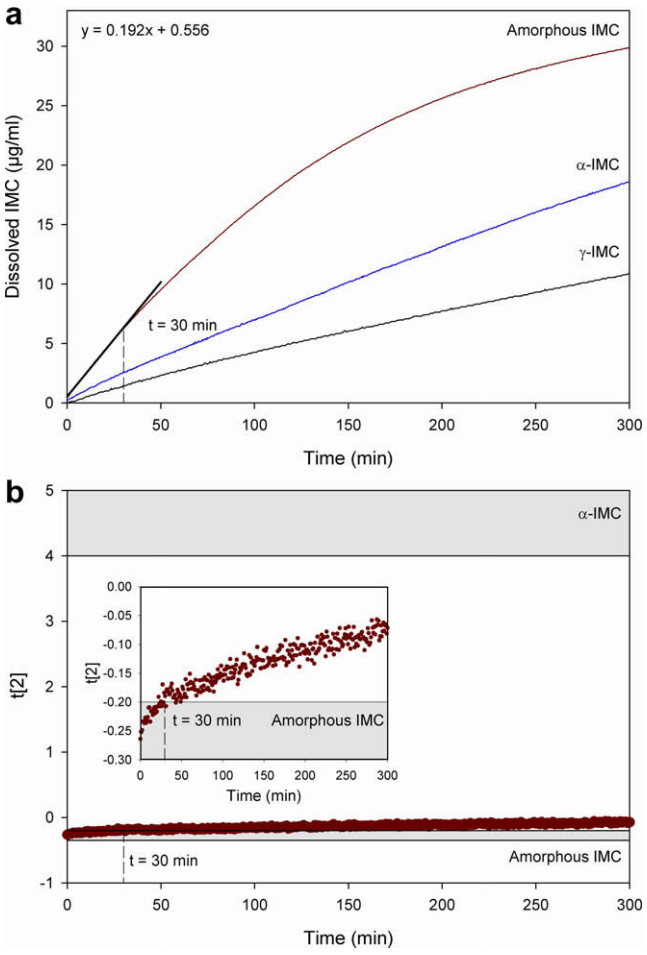

Fig. 4. (a) Dissolution of IMC in the phosphate buffer (pH 7.2) solution and (b) the respective scores of the amorphous sample following the PLS-DA. The grey areas represent the score regions (the area between smallest and largest score value) of amorphous IMC and crystalline α-IMC. The maximum standard deviation in concentrations is 2 µg/ml. The equation refers to the line of fit for the initial dissolution profile.

The yellow colour of the amorphous IMC causes fluorescence in the samples, which makes the analysis of the spectral data more difficult. Fluorescence causes an increase in the baseline, which masks the peaks in the spectra. To reduce the effects of fluorescence the samples were bleached before the experiment. The regions used to build the model were chosen so that the baseline effects caused by fluorescence, sample density differences and particle size could be mainly explained by a single factor. Thus, only the regions of 1085 to 1480 cm^{-1} and 1590 to 1690 cm^{-1} were chosen for the analysis. By choosing these regions for the PLS-DA, a model with two factors could be built. The R^2X, R^2Y and Q^2Y values were 98.5%, 99.4%, and 99.3%, respectively. R^2X explains the spectral variation included in the model, R^2Y explains how well the used data predict the different classes (solid-state forms) and Q^2Y is the test-set validation coefficient. In this model, the first factor was able to separate the amorphous samples from the crystalline ones (Fig. 5a). Also most of the baseline effects due to, for example, fluorescence and sample density or particle size differences were explained with the first factor. For example looking at the measured spectra and the score values for the first factor, the decrease in fluorescence in the amorphous samples caused the score values to increase towards zero. A second factor was needed to separate the crystalline α- (positive relationship) and γ-forms (negative relationship) from each other and the amorphous form. Thus, the second factor that explained 35.9% of the spectral variation could be used alone to describe the phase transition that occurred during the dissolution testing. Based on the weights plot, both the spectral regions used to build the PLS-DA model were equally important for the differentiation of the three solid-state forms (Fig. 5b). In these spectral regions, characteristic peaks largely due to delocalized ring deformations at 1085 to 1200 cm^{-1} as well as C=O stretching and indole ring deformations at 1590 to 1690 cm^{-1} are seen (Figs. 1a and 5b) [28,29].

PLS-DA does not enable the quantification of the crystallinity but the scores can be used to monitor the solid-state changes. PLS-DA of the Raman spectra was in agreement with the conclusions made based on the dissolution profiles and XRPD data. In both dissolution media the sample crystallized to the α-form, since in both the cases the scores of the second factor moved towards the α-form (Figs. 3 b and 4b). However, when phosphate buffer was used as the dissolution medium, even after a five hour experiment the scores still remained close to the score region of the pure amorphous form. This could be due to the sampling depth of the Raman probe. The sampling depth is probably a few hundred micrometers and somewhat deeper for the amorphous than crystalline material. Even though there was a thin layer of crystalline IMC on the outermost surface of the sample, the laser was penetrating through it and Raman scattering was detected from both the crystallized

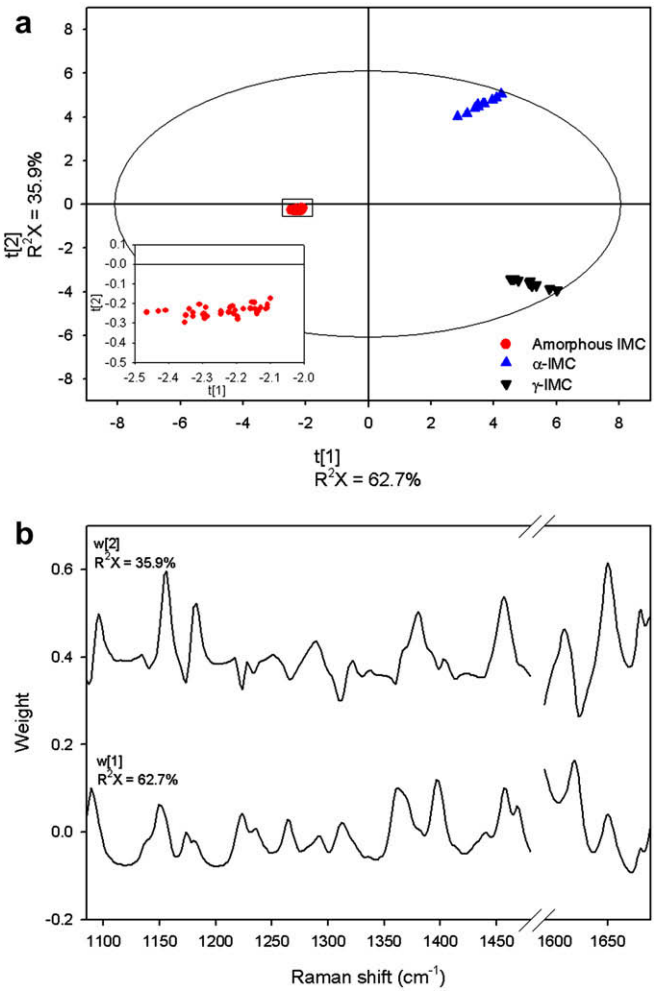

Fig. 5. (a) Scores plot of the amorphous, α- and γ-IMC and (b) the weights plot. Weights are offset for clarity.

surface and the amorphous sample that remained below the surface. A similar problem was noted when solid-phase transformations during dissolution of nitrofurantoin were evaluated [16]. The situation could be improved by using more surface sensitive methods, where the laser could be better focused on the outermost layer of the sample.

In phosphate buffer solution only the outermost surface of the sample crystallized during the dissolution experiment. A previous study has shown the surface crystallization rate of amorphous IMC below the T_g to be about two orders of magnitude faster than the bulk crystallization rate [30]. This could explain the slow crystallization of amorphous IMC below the surface of the sample in this study. Another important factor is that the absorption of water increases the molecular mobility of amorphous IMC, decreases the T_g of amorphous IMC and increases the overall crystallization rate [31,32]. The contact of the surface with the dissolution medium would, thus, decrease the T_g and increase the molecular mobility on the surface. This would increase the crystallization rate of the amorphous drug on the surface even more compared to the bulk crystallization rate and explain the faster surface crystallization rate noted in this study. Another possibility is that the crystallization process is solution-mediated. However, this would require a supersaturated solution [6]. The maximum solubility reported in the literature for IMC is 0.77 mg/ml in buffered aqueous media (pH 7.2) at 25 °C [33]. In this study, the maximum measured concentrations were about 0.03 mg/ml, which was less than 4% of the saturation concentration. Even though the amount of IMC in the solution is well below the saturation solubility, it is possible that the solution adjacent to the sample is supersaturated. Dissolved IMC could, thus, crystallize on the surface of the amorphous sample. At the end of the dissolution experiment, the dissolution rate of the amorphous sample in the phosphate buffer decreased below that of the crystalline counterparts, which could indicate the presence of saturated solution.

The PLS-DA analysis also verified the onset of crystallization to be less than two minutes in water–ethanol mixture and about 30 min in phosphate buffer solution as at these time points the scores moved away from the amorphous region. The advantage in using Raman spectroscopy in combination with the PLS-DA is that solid-state transitions that could not be detected with XRPD could be noted. PLS-DA of the Raman spectra also showed that the amorphous IMC crystallized directly to the α-form in both dissolution media. The crystallization of amorphous IMC to the α-form in buffer solution is in agreement with other studies, since amorphous IMC crystallizes to the α-form in high humidity conditions [31]. Lower humidity conditions, on the other hand, favour the formation of the γ-form.

3.2. Carbamazepine

3.2.1. Dissolution experiments

All CBZ samples were amorphous after the preparation based on the XRPD analysis (Fig. 6). However, two types of dissolution profiles were obtained from the amorphous samples (Fig. 7). Unlike with amorphous IMC, the release rate of CBZ was constant from the amorphous samples as well as the dihydrate tablets, and no significant improvement on the dissolution rates was noted. Dissolution from most of the amorphous samples was even slightly slower than from the dihydrate compacts (dissolution curve A in Fig. 7). However, in two experiments the dissolution was faster from the amorphous samples than from the dihydrate tablets (dissolution curve B in Fig. 7). XRPD analysis of the remaining sample after the dissolution experiment confirmed that the sample surface had converted to the dihydrate during all experiments (Fig. 6).

3.2.2. Monitoring the solid-state transformations

CBZ is known to exist as a dihydrate and four different anhydrate forms (I–IV), with the two principal forms being I (triclinic) and III (P-monoclinic) [19]. There is some inconsistency in the naming of the CBZ polymorphs in the literature. In this study,

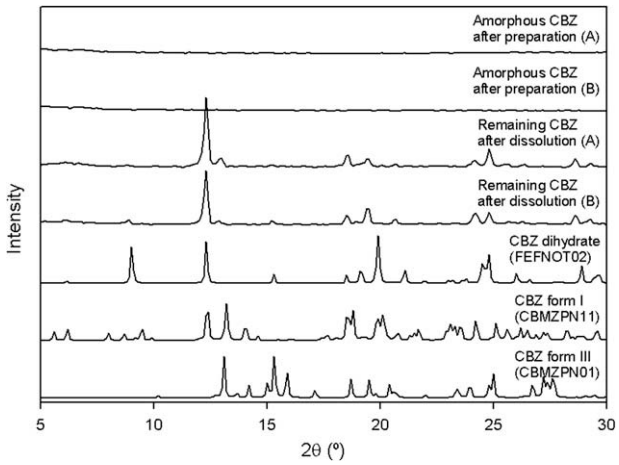

Fig. 6. XRPD patterns of the originally amorphous CBZ samples before and after the dissolution experiments and the theoretical diffraction patterns of the crystalline forms.

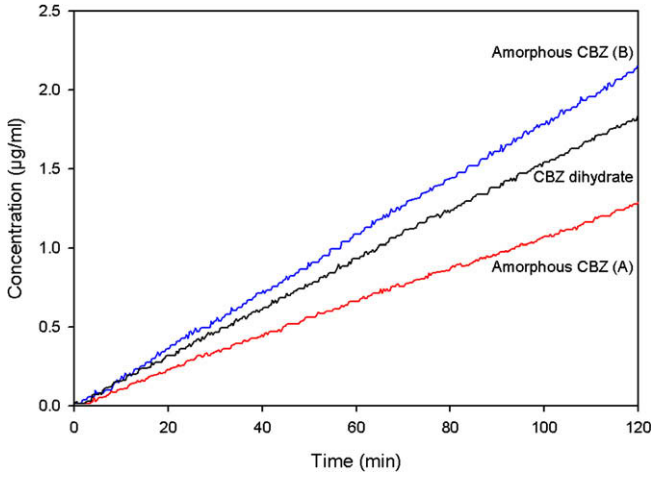

Fig. 7. Dissolution of CBZ in the phosphate buffer (pH 7.2) solution. Maximum standard deviation is 0.2 µg/ml. A and B are used in the text to refer to samples with lower and higher dissolution rates.

the same nomenclature is used as that reported by Grzesiak et al. [19].

Amorphous CBZ has been reported to crystallize to several anhydrate forms, as well as, the dihydrate depending on the environmental and processing conditions [34–36]. Amorphous anhydrous CBZ crystallized to form I (γ-CBZ according to Li et al. [34]) at temperatures below its T_g of 56 °C [19,34]. Immediately, after the preparation a quench-cooled amorphous CBZ crystallized to form I during DSC experiments [36]. However, after storing these samples at 25 °C at 75% RH for one week forms III, IV (form II according to Patterson et al. [36]) and dihydrate were observed. Grinding the dihydrate form in a ball mill resulted in the formation of amorphous CBZ [35]. The amorphous CBZ crystallized to the monoclinic form III (form I according to Otsuka et al. [35]) in both high and low humidity conditions. However, forms I and III are the most commonly reported anhydrates in the literature and, thus, in this study these, as well as the amorphous and the dihydrate forms, were included in the spectral analysis.

Raman spectroscopy is sensitive to the changes in intramolecular conformations and intermolecular interactions originating from solid-state structure changes. Although the Raman spectra of the different CBZ forms are very similar, small changes in the peak positions and intensities can be observed [24]. Multivariate analysis is, therefore, a good technique for analyzing the Raman spectra of CBZ, as the interpretation of the spectral changes due to solid-state transformations would otherwise be difficult. Three factors were needed to build a PLS-DA model of the Raman spectra that had R^2X, R^2Y, and Q^2Y values of 99.2%, 99.9% and 99.9%, respectively. The first factor was able to separate all forms to different clusters ($R^2X = 69.3\%$) (Fig. 8a). However, form III and dihydrate (positive relationship) were located quite near each other as well as amorphous and form I (negative relationship). The addition of the second factor ($R^2X = 22.4\%$) improved the differentiation of form III (positive relationship) from the dihydrate and the third factor ($R^2X = 7.5\%$) separated the amorphous CBZ from form I. The differentiation of the solid-state forms was mainly based on the differences in the spectral region 1500 to 1650 cm^{-1} for the first and third factors (Fig. 8b). In that region characteristic peaks of the stretching within the aromatic and $CONH_2$ groups are noted (Fig. 1b) [37,38]. Whereas for the second factor, the characteristic peaks in the spectral region 1200 to 1330 cm^{-1} were also significant, such as the deformations of the three ring structures and some stretching of the tertiary amide [37].

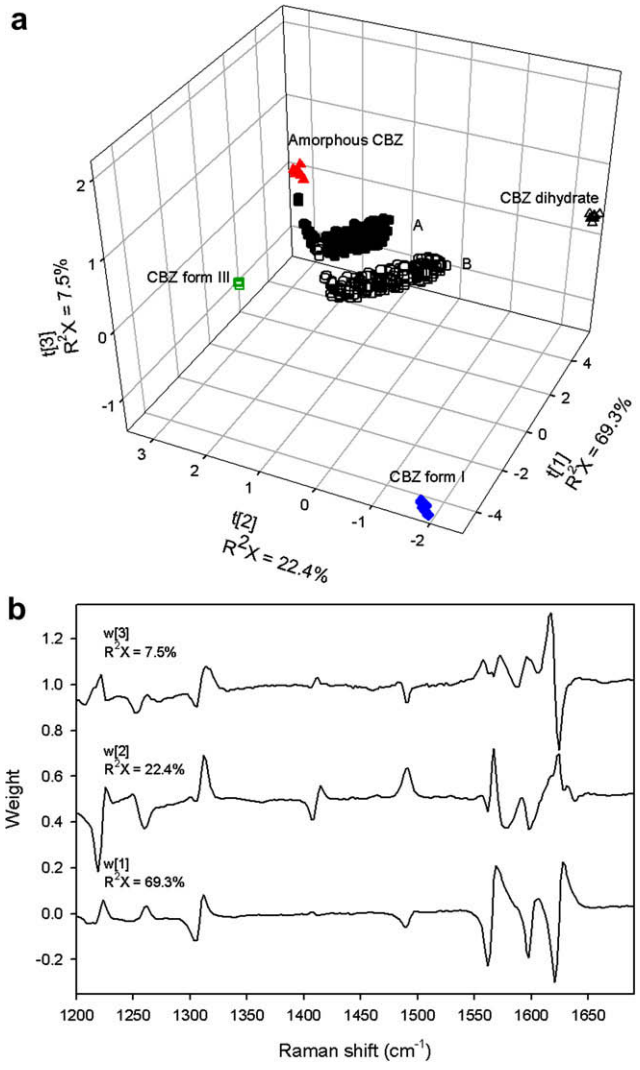

Fig. 8. (a) The PLS-DA model for the CBZ samples and scores for the amorphous CBZ samples following the PLS-DA of the Raman spectra measured during dissolution experiments. The scores for the samples with slower dissolution (A) are marked with symbol (●) and for the faster dissolution (B) with symbol (o). (b) The respective weights plot.

The PLS-DA of the Raman spectra measured *in situ* confirmed the surface crystallization of the samples, the surface of the sample started to crystallize immediately (Fig. 8). During the dissolution experiments, the scores started to move instantly out of the amorphous region towards the anhydrate form I and then later towards the dihydrate form. Thus, it seems that the amorphous CBZ does not crystallize directly to the dihydrate during the dissolution experiment. Instead, first a transition occurs from the amorphous form to crystalline anhydrate (form I) and then a solution-mediated transformation from form I to dihydrate [9]. The transition from the amorphous form to the crystalline anhydrate is likely a solid-state transition as amorphous CBZ has been shown to crystallize to an anhydrate form in dry conditions (25 °C and <10% RH) [36]. A difference could be noted in how far towards the form I the scores moved. The scores of the amorphous samples that had a higher dissolution rate (marked with B in Fig. 8) moved closer towards the scores region of form I than the scores of the amorphous samples that had a lower dissolution rate (marked with A in Fig. 8).

The faster dissolution from some of the originally amorphous samples is probably due to larger amounts of form I crystallizing in the samples as the scores are located nearer to the scores of form

I. Several studies have confirmed the dissolution rates of the crystalline forms to be of the order: form I > form III > dihydrate [9,39,40]. Even though all samples appeared X-ray amorphous after preparation, it is possible due to the preparation process of the amorphous CBZ that some nuclei or nanocrystalline material still remained in the samples or the sample had already crystallized before the start of the experiment. Forms I and III are enantiotropic, with form III being stable at temperatures below 71 °C [41]. Thus, based on Ostwald's step rule, form I would tend to form, when a melt is cooled down [2]. We confirmed this with XRPD by measuring a melted amorphous sample that had partly crystallized immediately after preparation (data not shown). Therefore, it is probable that if nuclei or small amounts of crystalline material were present in the X-ray amorphous samples, they would be of form I. When in contact with the dissolution medium, these samples would then be more likely to first crystallize to form I before converting to the dihydrate. The slower dissolution rate from the other originally amorphous samples compared to the dihydrate is most likely due to smaller specific surface area and wetting characteristics. The dihydrate samples were made from powder that was compressed to tablets, whereas the amorphous samples composed of one solid block.

3.2.3. Quantification of different solid-state forms

As the Raman spectra of the different solid-state forms of CBZ are very similar, a univariate or bivariate approach cannot be used for quantification. A multivariate approach has been used previously in our research group to quantify the different solid-state forms of CBZ appearing during dehydration [15]. In this study, this model was modified by including unground amorphous samples in the model, and was then applied to the Raman spectra gathered during the dissolution experiments of amorphous CBZ. In addition, a fifth PLS factor was included in the model. The dissolution medium flowing over the sample increased the noise level of the spectra gathered during the dissolution test compared to the spectra used in the calibration model. The addition of the fifth PLS factor improved the model performance (Fig. 9). Although the weights for this factor appear noisy, there still appears to be some systematic variation correlated with the sample concentrations. The model created had R^2X, R^2Y, and Q^2Y values of 97.0%, 96.2%, and 95.5%, respectively. In PLS analysis, the R^2Y explains how well the data in the **X** matrix (spectra) predict the **Y** matrix (concentrations). The root mean square errors of prediction set (RMSEPs) for the amorphous CBZ, form I, form III, and the dihydrate were 7.4%, 6.0%, 6.5%, and 2.4%, respectively. Even though the model was modified slightly, the scores plot and the observed vs. predicted concentrations were similar to those in the study by Kogermann et al. [15] and are, thus, not shown here.

The results supported the previous findings from the XRPD analysis and the PLS-DA of the Raman spectra. The amount of dihydrate formed at the end of the experiment was higher in the samples that had a higher dissolution rate (marked with B in Fig. 7) as about 35% of the surface had converted to the dihydrate and only about 25% had converted in the samples with a lower dissolution rate (marked with A in Fig. 7) (Fig. 10). As discussed in Section 3.1.2, some Raman scattering slightly below the surface is also detected. Thus, the uncrystallized sample below the surface affects the quantification. It is, therefore, likely that the amount of CBZ converted to the dihydrate on the surface was underestimated. CBZ dihydrate was formed on the surface of all the amorphous samples during the dissolution experiments. However, at the beginning of the dissolution experiment, more anhydrate form I crystallized in the samples where the dissolution was faster (marked with B in Fig. 7) (Fig. 10). The small amounts of crystalline residue in these samples functioned as seeds for crystallization and thus, induced crystal growth. Since form I is known to convert to the dihydrate in an aqueous environment [9], more dihydrate was also formed in these samples than the other originally amorphous samples (marked with A). Both the form I and the dihydrate have a needle-like morphology [42,43], and consequently the

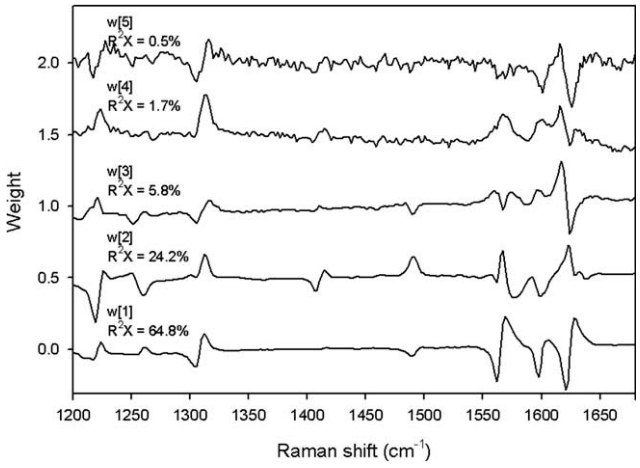

Fig. 9. The weights plot for the CBZ PLS model. Weights are offset for clarity.

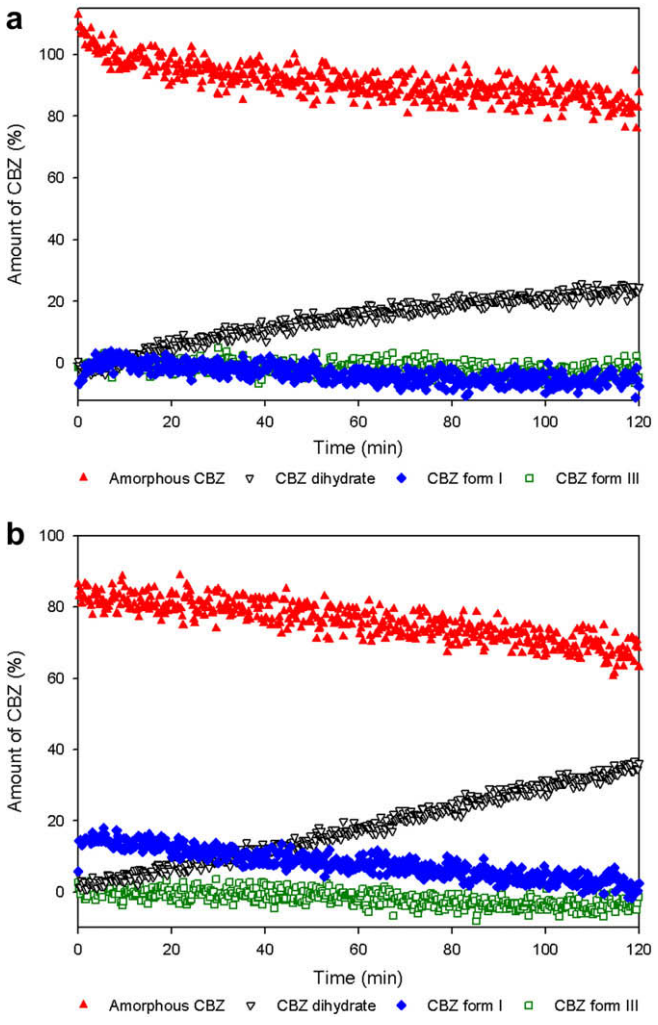

Fig. 10. The amount of different solid-state forms of CBZ appearing during the dissolution experiments based on the PLS regression analysis: (a) slower dissolution (A) and (b) faster dissolution (B).

appearance of these needle-like crystals on the amorphous sample surface increased the specific surface area. The crystalline layer formed on the sample surface, where water can penetrate and dissolve the drug, was thus thicker in samples marked with B. A previous study has shown that an increase in the specific surface area due to crystal growth increased the dissolution rate of CBZ dihydrate significantly [42]. This increase in the specific surface area could, thus, explain the higher dissolution rate observed from these samples.

A slight increase in the amount of form I could also be observed in the amorphous samples that had a lower dissolution rate. However, it is not possible to definitely say whether the amorphous form in these samples also initially crystallized to form I due to the RMSEP for quantification of form I being 6.0%. Nonetheless, the PLS-DA findings support this assumption that during dissolution in an aqueous environment the amorphous CBZ crystallizes first to the anhydrate form I through a solid-state transformation and then transforms to the dihydrate via a solution-mediated transformation. Amorphous CBZ converts to the CBZ dihydrate in aqueous solution [9]. However, to our knowledge the crystallization pathway has not been reported previously. Several studies confirm the transformation of both the anhydrate forms I and III to the dihydrate during dissolution experiments [9,39,44,45]. This conversion from the anhydrate to the dihydrate is a solution-mediated phase transformation [9].

4. Conclusion

There is an increasing interest in formulation approaches to improve the dissolution rate of poorly soluble drugs. Formulating the drug in an amorphous form is often presented as a possibility to try to improve dissolution properties of poorly soluble drugs. However, if the amorphous form transforms to a crystalline form during dissolution, the advantage is lost as the dissolution rate will gradually change to that of the crystalline form. This phenomenon was observed for both IMC and CBZ. However, IMC had slow crystallization kinetics and therefore, preparation of the amorphous form still improved the dissolution rate.

In situ Raman spectroscopy combined with multivariate techniques, such as PLS regression analysis and PLS-DA, offers a deeper insight into the phenomena that occur during the dissolution of amorphous materials. It is a fast and convenient way to detect the solid-state changes happening on the surface of the drug product during dissolution testing. Furthermore, multivariate techniques combined with Raman spectroscopy can be used to monitor the changes in the solid-state that remain unnoticed with XRPD.

References

[1] N. Blagden, M. de Matas, P.T. Gavan, P. York, Crystal engineering of active pharmaceutical ingredients to improve solubility and dissolution rates, Adv. Drug. Del. Rev. 59 (2007) 617–630.

[2] D.J.W. Grant, Theory and origin of polymorphism, in: H.G. Brittain (Ed.), Polymorphism in Pharmaceutical Solids, Marcel Dekker, New York, USA, 1999, pp. 1–33.

[3] L.F. Huang, W.Q. Tong, Impact of solid state properties on developability assessment of drug candidates, Adv. Drug Del. Rev. 56 (2004) 321–334.

[4] B.C. Hancock, M. Parks, What is the true solubility advantage for amorphous pharmaceuticals?, Pharm Res. 17 (2000) 397–404.

[5] S.R. Byrn, R.R. Pfeiffer, J.G. Stowell, Solid-state Chemistry of drugs, second ed., SSCI, Inc., West Lafayette, IN, USA, 1999.

[6] G.G.Z. Zhang, D. Law, E.A. Schmitt, Y. Qiu, Phase transformation considerations during process development and manufacture of solid oral dosage forms, Adv. Drug Del. Rev. 56 (2004) 371–390.

[7] T. Wu, Y. Sun, N. Li, M.M. de Villiers, L. Yu, Inhibiting surface crystallization of amorphous indomethacin by nanocoating, Langmuir 23 (2007) 5148–5153.

[8] M. Yoshioka, B.C. Hancock, G. Zografi, Crystallization of indomethacin from the amorphous state below and above its glass transition temperature, J. Pharm. Sci. 83 (1994) 1700–1705.

[9] D. Murphy, F. Rodriguez-Cintron, B. Langevin, R.C. Kelly, N. Rodriguez-Hornedo, Solution-mediated phase transformation of anhydrous to dihydrate carbamazepine and the effect of lattice disorder, Int. J. Pharm. 246 (2002) 121–134.

[10] S. Debnath, P. Predecki, R. Suryanarayanan, Use of glancing angle X-ray powder diffractometry to depth-profile phase transformations during dissolution of indomethacin and theophylline tablets, Pharm. Res. 21 (2004) 149–159.

[11] E. Fukuoka, M. Makita, S. Yamamura, Some physicochemical properties of glassy indomethacin, Chem. Pharm. Bull. 34 (1986) 4314–4321.

[12] Y. Chikaraishi, M. Otsuka, Y. Matsuda, Dissolution phenomenon of the piretanide amorphous form involving phase change, Chem. Pharm. Bul. 44 (1996) 2111–2115.

[13] N. Kaneniwa, M. Otsuka, T. Hayashi, Physicochemical characterization of indomethacin polymorphs and the transformation kinetics in ethanol, Chem. Pharm. Bull. 33 (1985) 3447–3455.

[14] C. Lefebvre, A. Guyot-Hermann, M. Draguet-Brughmans, R. Bouche, Dissolution rate and polymorphism of carbamazepine: study of different specialities, Pharm. Acta Helv. 62 (1987) 341–347.

[15] K. Kogermann, J. Aaltonen, C.J. Strachan, K. Pöllänen, J. Heinämäki, J. Yliruusi, J. Rantanen, Establishing quantitative in-line analysis of multiple solid-state transformations during dehydration, J. Pharm. Sci., in press.

[16] J. Aaltonen, P. Heinänen, L. Peltonen, H. Kortejärvi, V.P. Tanninen, L. Christiansen, J. Hirvonen, J. Yliruusi, J. Rantanen, In situ measurement of solvent-mediated phase transformations during dissolution testing, J. Pharm. Sci. 95 (2006) 2730–2737.

[17] X. Chen, K.R. Morris, U.J. Griesser, S.R. Byrn, J.G. Stowell, Reactivity differences of indomethacin solid forms with ammonia gas, J. Am. Chem. Soc. 124 (2002) 15012–15019.

[18] P.J. Cox, P.L. Manson, γ-Indomethacin at 120 K, Acta Crystallogr. E (2003).

[19] A.L. Grzesiak, M. Lang, K. Kim, A.J. Matzger, Comparison of the four anhydrous polymorphs of carbamazepine and the crystal structure of form I, J. Pharm. Sci. 92 (2003) 2260–2271.

[20] J.P. Reboul, B. Cristau, J.C. Soyfer, J.P. Astier, 5H-Dibenz[*b*,*f*]-azepinecarboxamide-5 (carbamazepine), Acta Crystallogr. B (1981).

[21] R. Harris, P. Ghi, H. Puschmann, D. Apperley, U. Griesser, R. Hammond, C. Ma, K. Roberts, G. Pearce, J. Yates, C. Pickard, Structural studies of the polymorphs of carbamazepine, its dihydrate, and two solvates, Org. Process Res. Dev. 9 (2005) 902–910.

[22] L. Eriksson, E. Johansson, N. Kettaneh-Wold, S. Wold, Multi- and megavariate data analysis. Principles and applications, Umetrics AB, Umea, 2001.

[23] R.J. Barnes, M.S. Dhanoa, S.J. Lister, Standard normal variate transformation and de-trending of near-infrared diffuse reflectance spectra, Appl. Spectrosc. 43 (1989) 772–777.

[24] K. Kogermann, J. Aaltonen, C.J. Strachan, K. Pollanen, P. Veski, J. Heinamaki, J. Yliruusi, J. Rantanen, Qualitative in situ analysis of multiple solid-state forms using spectroscopy and partial least squares discriminant modeling, J. Pharm. Sci. 96 (2007) 1802–1820.

[25] E. Fukuoka, M. Makita, S. Yamamura, Glassy state of pharmaceuticals. II. Bioinequivalence of glassy and crystalline indomethacin, Chem. Pharm. Bull. 35 (1987) 2943–2948.

[26] H. Imaizumi, N. Nambu, T. Nagai, Stability and several physical properties of amorphous and crystalline forms of indomethacin, Chem. Pharm. Bull. 28 (1980) 2565–2569.

[27] A. Heinz, M. Savolainen, T. Rades, C.J. Strachan, Quantifying ternary mixtures of different solid-state forms of indomethacin by Raman and near-infrared spectroscopy, Eur. J. Pharm. Sci. (2007).

[28] M. Savolainen, A. Heinz, C. Strachan, K.C. Gordon, J. Yliruusi, T. Rades, N. Sandler, Screening for differences in the amorphous state of indomethacin using multivariate visualization, Eur. J. Pharm. Sci. 30 (2007) 113–123.

[29] C.J. Strachan, T. Rades, K.C. Gordon, A theoretical and spectroscopic study of gamma-crystalline and amorphous indometacin, J. Pharm. Pharmacol. 59 (2007) 261–269.

[30] T. Wu, L. Yu, Surface crystallization of indomethacin below T_g, Pharm. Res. 23 (2006) 2350–2355.

[31] V. Andronis, M. Yoshioka, G. Zografi, Effects of sorbed water on the crystallization of indomethacin from the amorphous state, J. Pharm. Sci. 86 (1997) 346–351.

[32] V. Andronis, G. Zografi, The molecular mobility of supercooled amorphous indomethacin as a function of temperature and relative humidity, Pharm. Res. 15 (1998) 835–842.

[33] A. Nokhodchi, Y. Javadzadeh, M.R. Siahi-Shadbad, M. Barzegar-Jalali, The effect of type and concentration of vehicles on the dissolution rate of a poorly soluble drug (indomethacin) from liquisolid compacts, J. Pharm. Pharm. Sci. 8 (2005) 18–25.

[34] Y. Li, J. Han, G.G.Z. Zhang, D.J.W. Grant, R. Suryanarayanan, In situ dehydration of carbamazepine dihydrate: a novel technique to prepare amorphous anhydrous carbamazepine, Pharm. Dev. Technol. 5 (2000) 257–266.

[35] M. Otsuka, T. Ofusa, Y. Matsuda, Effect of environmental humidity on the transformation pathway of carbamazepine polymorphic modifications during grinding, Colloids Surf. B Biointerfaces 13 (1999) 263–273.

[36] J.E. Patterson, M.B. James, A.H. Forster, R.W. Lancaster, J.M. Butler, T. Rades, The influence of thermal and mechanical preparative techniques on the amorphous state of four poorly soluble compounds, J. Pharm. Sci. 94 (2005) 1998–2012.

[37] L.E. O'Brien, P. Timmins, A.C. Williams, P. York, Use of in situ FT-Raman spectroscopy to study the kinetics of the transformation of carbamazepine polymorphs, J. Pharm. Biomed. Anal. 36 (2004) 335–340.
[38] C.J. Strachan, S.L. Howell, T. Rades, K.C. Gordon, A theoretical and spectroscopic study of carbamazepine polymorphs, J. Raman Spectrosc. 35 (2004) 401–408.
[39] Y. Kobayashi, S. Ito, S. Itai, K. Yamamoto, Physicochemical properties and bioavailability of carbamazepine polymorphs and dihydrate, Int. J. Pharm. 193 (2000) 137–146.
[40] Y. Yoshihashi, E. Yonemochi, K. Terada, Estimation of initial dissolution rate of drug substance by thermal analysis: application for carbamazepine hydrate, Pharm. Dev. Technol. 7 (2002) 89–95.
[41] R.J. Behme, D. Brooke, Heat of fusion measurement of a low melting polymorph of carbamazepine that undergoes multiple-phase changes during differential scanning calorimetry analysis, J. Pharm. Sci. 80 (1991) 986–990.
[42] F. Tian, N. Sandler, J. Aaltonen, C. Lang, D.J. Saville, K.C. Gordon, C.J. Strachan, J. Rantanen, T. Rades, Influence of polymorphic form, morphology, and excipient interactions on the dissolution of carbamazepine compacts, J. Pharm. Sci. 96 (2007) 584–594.
[43] F. Tian, J.A. Zeitler, C.J. Strachan, D.J. Saville, K.C. Gordon, T. Rades, Characterizing the conversion kinetics of carbamazepine polymorphs to the dihydrate in aqueous suspension using Raman spectroscopy, J. Pharm. Biomed. Anal. 40 (2006) 271–280.
[44] P. Kahela, R. Aaltonen, E. Lewing, M. Anttila, E. Kristoffersson, Pharmacokinetics and dissolution of two crystalline forms of carbamazepine, Int. J. Pharm. 14 (1983) 103–112.
[45] E. Laine, V. Tuominen, P. Ilvessalo, P. Kahela, Formation of dihydrate from carbamazepine anhydrate in aqueous conditions, Int. J. Pharm. 20 (1984) 307–314.